Monthly Notices of the ROYAL ASTRONOMICAL SOCIETY

MNRAS **546,** 1–8 (2026) https://doi.org/10.1093/mnras/stag029
Advance Access publication 2026 January 08

Auriga Streams III: the mass–metallicity relation does not rule out tidal mass-loss in Local Group satellites

Alexander H. Riley [1,2★] Rebekka Bieri [3] Alis J. Deason [1] Nora Shipp [4] Christine M. Simpson [5] Francesca Fragkoudi [1] Facundo A. Gómez [6] Robert J. J. Grand [7] and Federico Marinacci [8,9]

[1]*Institute for Computational Cosmology, Department of Physics, Durham University, South Road, Durham DH1 3LE, UK*
[2]*Lund Observatory, Division of Astrophysics, Department of Physics, Lund University, SE-221 00 Lund, Sweden*
[3]*Department of Astrophysics, University of Zurich, CH-8057 Zurich, Switzerland*
[4]*Department of Astronomy, University of Washington, Seattle, WA 98195, USA*
[5]*Argonne Leadership Computing Facility, Argonne National Laboratory, Lemont, IL 60439, USA*
[6]*Departamento de Astronomía, Universidad de La Serena, Av. Juan Cisternas 1200 Norte, La Serena, Chile*
[7]*Astrophysics Research Institute, Liverpool John Moores University, 146 Brownlow Hill, Liverpool L3 5RF, UK*
[8]*Department of Physics & Astronomy 'Augusto Righi', University of Bologna, via Gobetti 93/2, I-40129 Bologna, Italy*
[9]*INAF, Astrophysics and Space Science Observatory Bologna, via P. Gobetti 93/3, I-40129 Bologna, Italy*

Accepted 2025 December 16. Received 2025 December 15; in original form 2025 September 11

ABSTRACT

The mass–metallicity relation is a fundamental galaxy scaling law that has been extended to the faintest systems in the Local Group. We show that the small scatter in this relation, which has been used to argue against tidal mass-loss in Local Group satellites, is consistent with the level of disruption in the Auriga simulations. For every accreted system in Auriga, we compute stellar masses and metallicities two ways: considering the total system (bound + lost material) and only considering the progenitor. Accreted systems in Auriga have a tight relation between total stellar mass and metallicity, with scatter at a fixed stellar mass driven by age. When only considering the progenitor, the tidally evolved mass–metallicity relation has similar scatter (∼0.27 dex) as observed for the Local Group satellites (∼0.23 dex). Satellites that lie above the evolved relation have experienced substantial mass-loss and typically have low metallicity for their total stellar mass. Even satellites that fall exactly on the evolved relation can lose over half of their stellar mass. Only satellites substantially below the evolved relation are reliably intact. Based on their offset from the observed relation, we predict which Milky Way and M31 satellites have tidal tails waiting to be discovered.

Key words: Galaxy: halo – galaxies: evolution – galaxies: formation – Local Group.

1 INTRODUCTION

The mass–metallicity relation is a fundamental scaling law connecting the stellar mass of a galaxy to its metal contents (e.g. C. A. Tremonti et al. 2004; L. J. Kewley & S. L. Ellison 2008; F. Mannucci et al. 2010; R. Maiolino & F. Mannucci 2019). The relation is governed by the complex interplay between star formation, stellar evolution, accretion, and baryonic feedback. It has been extended to the faintest galaxies within the Local Volume (J. D. Simon & M. Geha 2007; E. N. Kirby et al. 2008, 2013, 2020), many of which are satellites of the Milky Way and M31.

The observed scatter[1] in this relation is remarkably small, ∼0.15 to 0.25 dex depending on adopted measurements. It is conventionally argued (e.g. J. D. Simon & M. Geha 2007; J. D. Simon 2019) that this small scatter indicates that the Local Group satellites have not experienced substantial mass-loss. This is because individual systems would move towards smaller mass and higher mean metallicity if the system begins with a negative radial metallicity gradient and low-metallicity stars in the outskirts are preferentially lost. This would tend to increase scatter in the correlation.

Many cosmological hydrodynamical zoom-in simulations of Milky Way-mass galaxies claim to match the mass–metallicity relation (A. Genina et al. 2019; E. Applebaum et al. 2021; R. J. J. Grand et al. 2021), often with similar or smaller scatter than the observations. Recent analyses of such simulations (N. Shipp et al. 2023, 2025; A. H. Riley et al. 2025) show that their satellites have experienced much more tidal disruption than previously understood. How do these simulations produce mass–metallicity relations with small scatter, despite such a high level of mass-loss? Is the observed mass–metallicity relation indicative of an intrinsic relation, or possibly one that has evolved due to tides?

Our goal in this work is to examine these questions using the Auriga simulations. We restrict our analysis to satellites

★ E-mail: alexander.riley@fysik.lu.se

[1]We adopt the RMSE, $\sigma_{\rm scatter} \equiv \left[\sum ([{\rm Fe/H}]_{\rm obs} - [{\rm Fe/H}]_{\rm model})^2 / N\right]^{1/2}$.

© The Author(s) 2026.
Published by Oxford University Press on behalf of Royal Astronomical Society. This is an Open Access article distributed under the terms of the Creative Commons Attribution License (https://creativecommons.org/licenses/by/4.0/), which permits unrestricted reuse, distribution, and reproduction in any medium, provided the original work is properly cited.

Downloaded from https://academic.oup.com/mnras/article/546/3/stag029/8417159 by guest on 27 February 2026

that reach $M_\star \gtrsim 5 \times 10^5$ M$_\odot$, excluding the ultrafaint systems that may not follow the same mass–metallicity relation (S. W. Fu et al. 2023) due to higher sensitivity to supernova feedback strength and other galaxy formation physics (O. Agertz et al. 2020).

2 DISRUPTING SATELLITES IN AURIGA

We use the suite of Milky Way-mass haloes from the Auriga project (R. J. J. Grand et al. 2017, 2024). These haloes were selected from the EAGLE dark-matter-only 100 Mpc box (J. Schaye et al. 2015) to have $M_{200c} = 1 - 2 \times 10^{12}$ M$_\odot$ and satisfy an isolation criterion. They were resimulated with the moving-mesh code AREPO (V. Springel 2010; R. Pakmor et al. 2016) and a galaxy formation model detailed in R. J. J. Grand et al. (2017, 2024). The Auriga model produces spiral disc galaxies that are broadly consistent with a number of observations including stellar masses, sizes, and rotation curves (R. J. J. Grand et al. 2017), H I gas distributions (F. Marinacci et al. 2017), stellar disc warps (F. A. Gómez et al. 2017), stellar bars (F. Fragkoudi et al. 2020, 2025), satellite galaxies (C. M. Simpson et al. 2018), stellar haloes (A. Monachesi et al. 2019), and magnetic fields (R. Pakmor et al. 2017). The simulations are described in further detail in R. J. J. Grand et al. (2017, 2024).

A. H. Riley et al. (2025) and N. Shipp et al. (2025), hereafter Paper I and Paper II, presented a uniform and complete catalogue of all systems that accreted onto the Milky Way-mass hosts in Auriga. In addition to identifying the star particles associated with each system, they also assessed which are bound to the progenitor at present day according to SUBFIND (V. Springel et al. 2001). They analysed three different numerical resolutions available in Auriga; we focus here on the six haloes that were simulated at 'level 3' resolution with baryonic element (dark matter particle) masses of $6.7(36)\times10^3$ M$_\odot$ and a minimum softening length of 188 pc. This resolution is sufficient to study accreted systems down to $M_\star \sim 5 \times 10^5$ M$_\odot$ with over 100 star particles.

The Auriga simulations trace individual abundances for nine elements: H, He, C, O, N, Ne, Mg, Si, and Fe. The abundances of individual star particles are inherited from the gas cell they are born from. We define the metallicity of a star particle as

$$[\mathrm{Fe/H}] = \log_{10}\left(\frac{M_\mathrm{Fe}}{M_\mathrm{H}}\right) - \log_{10}\left(\frac{55.845}{1.008}\right) - (7.46 - 12), \quad (1)$$

where M_X is the ratio of mass in species X to the total mass of the parent gas cell, the second term converts mass to number density using the atomic mass of each species, and the third term sets $[\mathrm{Fe/H}]_\odot \equiv 0$ (M. Asplund, A. M. Amarsi & N. Grevesse 2021). When computing the mean metallicities for an accretion event, we follow conventions for resolved star observations in the Local Group. In particular, we weight each star particle by its present-day stellar mass and compute the mean of [Fe/H] as defined in equation (1) (see section 3.1 of I. Escala et al. 2018). For each system[2] we compute the mean metallicity two ways: across all stars formed in that system ('total') and only those bound to the progenitor ('bound'). We refer to the resulting mass–metallicity relations as 'intrinsic' and '(tidally) evolved', respectively. We denote the fraction of total stellar mass that remains bound to the progenitor as f_bound[3]

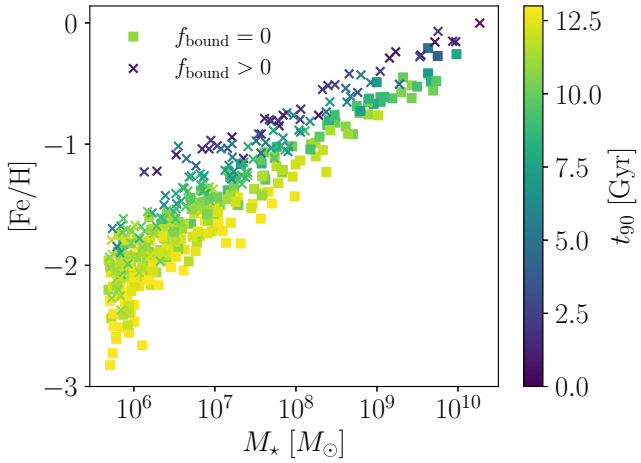

Figure 1. The intrinsic mass–metallicity relation for accreted systems in Auriga. Squares indicate systems that have been fully disrupted ($f_\mathrm{bound} = 0$) while crosses indicate systems that still have a bound progenitor at the present day ($f_\mathrm{bound} > 0$). The scatter at fixed total stellar mass is driven by age (colour of points), parametrized here as t_{90}.

We caution that the Auriga model produces central galaxies, satellites, and stellar haloes that are more metal-rich than in observations (A. Monachesi et al. 2019; R. J. J. Grand et al. 2021; N. Kizhuprakkat et al. 2024). We focus on the evolution of the mass–metallicity relation as Auriga satellites lose stellar mass, which depends on *relative* changes. In Section 4, we compare the offsets from the mass–metallicity relation for both Auriga and observations, but only after normalizing by the scatter about their respective relations, which also mitigates this issue. Similarly, if satellites in Auriga disrupt too readily (either from numerical resolution or unrealistic physical properties), the general qualitative trends reported in this work should still hold.

3 INTRINSIC VERSUS EVOLVED MASS–METALLICITY RELATION

In Fig. 1, we present the intrinsic mass–metallicity relation for all accreted systems in Auriga, regardless of whether or not they have a bound progenitor at the present day. The scatter at fixed total stellar mass is driven by age[4]; older objects at a given stellar mass have lower metallicity and are more likely to be fully disrupted. This naturally arises from a mass–metallicity relation that evolves with redshift due to self enrichment (e.g. X. Ma et al. 2016; P. Torrey et al. 2019), combined with environmental quenching and tidal disruption experienced by objects from a cosmological accretion history. We also find that fully disrupted systems have higher [α/Fe] than those that survive to the present day, a familiar result in both simulations (B. Robertson et al. 2005; A. S. Font et al. 2006; A. Fattahi et al. 2020; S. E. Grimozzi, A. S. Font & M. E. De Rossi 2024; D. Pathak et al. 2025) and observations (A. P. Ji et al. 2020; S. Hasselquist et al. 2021; R. P. Naidu et al. 2022) that is driven by the same physical processes.

[2]We remove 13 systems (of 419 total) that are phase-mixed with intrinsic $M_\star \lesssim 10^7$ M$_\odot$ and [Fe/H] $\gtrsim -0.9$. These are contaminated by merger-driven starbursts, becoming outliers in mass–metallicity–age.

[3]We refer to sections 1 and 3 of Paper I for adopted nomenclature and definitions (e.g. 'bound', 'progenitor', 'total stellar mass' of a system).

[4]Parametrized as the lookback time by which 90 per cent of stellar mass formed and denoted as t_{90}.

Downloaded from https://academic.oup.com/mnras/article/546/3/stag029/8417159 by guest on 27 February 2026

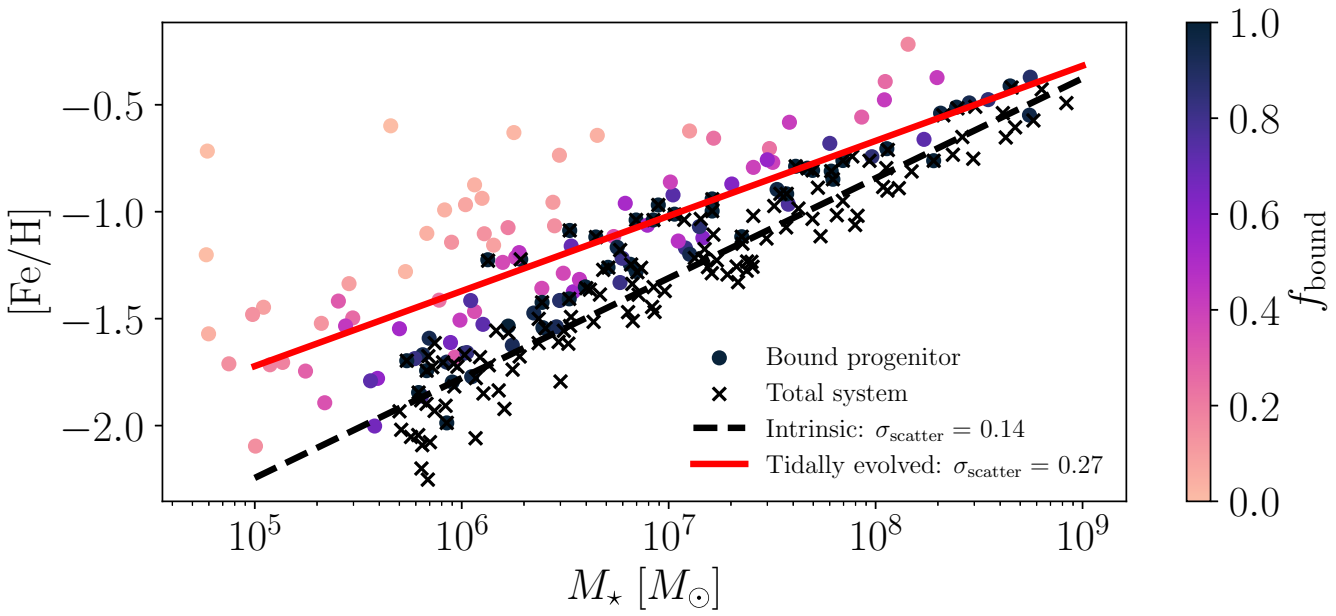

Figure 2. The intrinsic and tidally evolved mass–metallicity relations for Auriga satellites that have $f_{\rm bound} > 0$. Individual systems are shown both considering bound progenitors (circles) and the total system (crosses). We provide linear fits to both bound (solid red) and total (dashed black) cases, along with the vertical scatter about these relations. We only include systems that have 10 or more bound star particles at the present day.

In Fig. 2, we present both the intrinsic and evolved mass–metallicity relations for surviving Auriga satellites (i.e. $f_{\rm bound} > 0$). Every satellite is represented in the figure twice: crosses indicate values when considering bound and lost material (at the same locations as in Fig. 1), while the circles only consider stars that remain bound to the progenitor at the present day. As satellites disrupt, they move towards lower (bound) stellar mass and higher mean metallicity. The increase in mean metallicity is a result of negative radial metallicity gradients in Auriga[5] (S. Khoperskov et al. 2023; M. D. A. Orkney et al. 2023; A. Carrillo et al. 2024) – as lower metallicity stars in the outer regions are removed first, the remaining bound progenitor has a higher mean metallicity than the overall system. We note that negative metallicity gradients are common in observed low-mass galaxies in the Local Group and beyond (E. N. Kirby et al. 2011; R. Leaman et al. 2013; S. Taibi et al. 2022; F. O. Barbosa et al. 2025).

We fit linear models to both the intrinsic and tidally evolved data for systems that have $f_{\rm bound} > 0$. Due to tidal mass-loss and negative metallicity gradients, the evolved relation sits higher and has a larger scatter (0.27) than the intrinsic relation (0.14). The tidally evolved relation, which only considers the bound progenitor, is the simulated analogue to the measurements reported in E. N. Kirby et al. (2013) and similar analyses.

The scatter in the tidally evolved relation is primarily driven by mass-loss. At fixed bound stellar mass, satellites with high $f_{\rm bound}$ are generally below the tidally evolved relation, while satellites with low $f_{\rm bound}$ are above this relation. Even satellites that fall exactly on the relation can lose substantial amounts of stellar mass. We also note that individual points 'invert' their relationship to the mass–metallicity relation. Satellites that have low $f_{\rm bound}$ move in the mass–metallicity plane from being below the intrinsic relation to being above the tidally evolved relation. Satellites that have high $f_{\rm bound}$ begin above the intrinsic relation and remain in the same location of the mass–metallicity plane, but the relation shifts such that they end up below the tidally evolved relation. There is a modest decrease in scatter about the tidally evolved relation with increasing stellar mass, while the scatter is more uniform for the intrinsic relation.

Finally, we note that there is a collection of satellites with $f_{\rm bound} \simeq 1$ that fall on or slightly above the tidally evolved relation. These systems are star forming, recently accreted satellites that have the highest possible metallicity for their total stellar mass (see Fig. 1). The agreement in mass–metallicity relations between different morphological classes of observed galaxies (E. N. Kirby et al. 2013) and between satellite and field galaxies in some simulations (E. Applebaum et al. 2021) may stem from comparing the intrinsic relation of recently accreted (or isolated) star forming systems to the tidally evolved relation of quiescent systems. We show these galaxies in Fig. 2 but exclude them elsewhere in this work.

4 THE LOCAL GROUP SATELLITES

In Section 3, we established a connection between how disrupted a satellite in Auriga is and where it sits in the mass–metallicity plane relative to the tidally evolved relation. Now we connect this result to the observed satellites of the Milky Way and M31. We consider satellites that are brighter than $M_V = -7.7$ (J. D. Simon 2019) and have literature [Fe/H] measurements derived from spectroscopy. We adopt values reported in A. B. Pace (2025) for all stellar mass measurements[6] and augment their spectroscopic measurements with values for high-mass satellites from either A. W. McConnachie (2012) or E. N. Kirby et al. (2013). Specific measurements and their original sources are listed in Appendix B.

[5]We discuss ignoring metallicity gradients in Appendix A.

[6]In practice, A. B. Pace (2025) take literature V-band luminosities and adopt a uniform $M_\star/L_V = 2$.

Downloaded from https://academic.oup.com/mnras/article/546/3/staq029/8417159 by guest on 27 February 2026

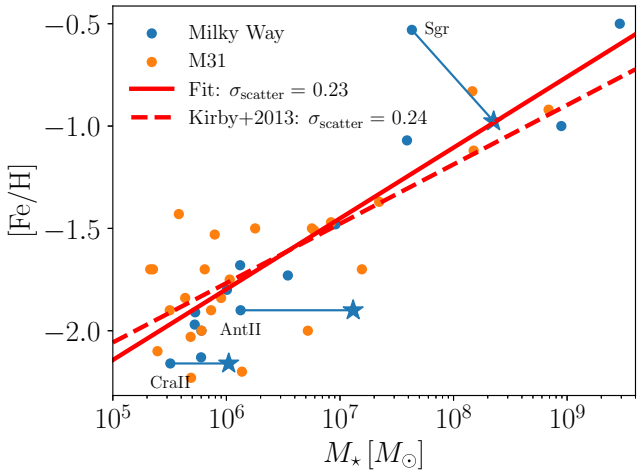

Figure 3. The mass–metallicity relation for observed satellites of the Milky Way (blue points) and M31 (orange points). We provide a linear fit to these satellites (solid) and the relation from E. N. Kirby et al. (2013) (dashed). We also highlight individual satellites known or believed to be disrupting and their reconstructed 'total' values (star symbols, see the text for details).

In Fig. 3, we present these measurements along with the relation reported in E. N. Kirby et al. (2013).[7] We note that the fit reported in E. N. Kirby et al. (2013) includes ultrafaint systems down to 10^3 $M_\odot$, which do not appear to continue the relation and instead flatten at [Fe/H] ~ -2.6 (S. W. Fu et al. 2023). For a consistent treatment, we fit a new relation as done for the Auriga satellites (Fig. 2). This fit reduces the scatter from 0.24 to 0.23, which is comparable to the 0.27 for bound satellites in Auriga. We emphasize that this is the first time a simulation has shown that a mass–metallicity relation with small scatter (comparable to observations) can still emerge from a system of satellites undergoing substantial tidal disruption.

We compute the vertical (i.e. at fixed mass) offset from the fit Δ[Fe/H] for each satellite, which is positive (negative) for satellites that sit above (below) the relation. In the top panel of Fig. 4, we present these offsets and show they broadly correlate with $f_{\rm bound}$ for the Auriga satellites, as seen in Fig. 2.

We can leverage this connection between $f_{\rm bound}$ and Δ[Fe/H] to predict which Local Group satellites are actively disrupting. This is detailed in Appendix B, but in brief, we assign a Class 1 through 5 based on the offset Δ[Fe/H] normalized by the $\sigma_{\rm scatter}$ about the relation. The boundaries between the different classes are shown as dashed lines in Fig. 4 and largely capture different categories of mass-loss in Auriga, from unlikely to be losing mass (Class 1) to guaranteed to have experienced extreme disruption (Class 5). In particular, we highlight the following quiescent systems predicted to be disrupting at high confidence:

(i) Class 3 ($0.05 < f_{\rm bound} < 0.8$): Fornax, Leo II, NGC 147, And I, II, III, VI, XIX, XXI, XXVIII, XXIX
(ii) Class 4 ($f_{\rm bound} < 0.2$): And XVII, And XVIII, Cassiopeia II
(iii) Class 5 ($f_{\rm bound} < 0.05$): Sagittarius, And XV

The offset Δ[Fe/H] and predicted disruption Class for individual Local Group satellites are reported in Appendix B.

[7]For consistency with our adopted stellar masses, we use the luminosity–metallicity relation reported in equation (3) of E. N. Kirby et al. (2013) and apply the same $M_\star/L_V = 2$.

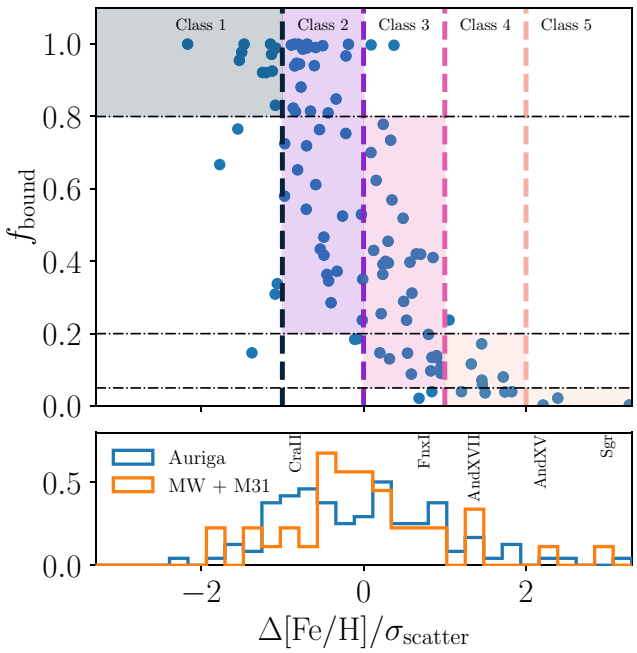

Figure 4. Top panel: $f_{\rm bound}$ versus scaled offset from the evolved mass–metallicity relation for Auriga satellites. The dashed lines are the boundaries between the five broad categories of mass-loss detailed in Section 4 and Appendix B. Bottom panel: histogram of scaled offsets for both Auriga and Milky Way and M31 satellites from their respective mass–metallicity relations.

It may appear surprising that so many Local Group satellites could be significantly disrupted, especially given current detections. However, the tidal tails emanating from these systems are likely too faint to be detected in current resolved-star imaging, so the satellites would appear intact (N. Shipp et al. 2023). These low surface brightness features may be visible by upcoming facilities including Rubin LSST, *Euclid*, and *Roman*.

To illustrate how far satellites can move in the mass–metallicity plane, in Fig. 3 (star symbols) we provide reconstructions of the 'total' system for three prominent examples of disrupting Milky Way satellites: Sagittarius, Antlia II, and Crater II. For Sagittarius we adopt an $f_{\rm bound} = 0.19$ (M. Niederste-Ostholt et al. 2010) and assume that the progenitor has mean [Fe/H] $= -0.58$, while the tails are more metal-poor with [Fe/H] $= -1.07$ (G. Limberg et al. 2022; E. C. Cunningham et al. 2024). For Antlia II and Crater II we adopt modelling estimates of $f_{\rm bound} = 0.1$ (O. Sameie et al. 2020) and 0.3 (J. L. Sanders, N. W. Evans & W. Dehnen 2018) respectively[8] and assume there is no shift in metallicity given the lack of a detected metallicity gradient (A. P. Ji et al. 2021).

Even though these estimates are simple, they illustrate (based on independent modeling) how far individual satellites can travel in the mass–metallicity plane. In addition, it is clear that their 'total' mass and metallicity should not be compared to the mass–metallicity relation of satellites, but to the (unknown) intrinsic relation (as highlighted in Fig. 2). It is also intriguing that these reconstructions move their respective satellites near the lowest

[8]A. P. Ji et al. (2021) argue against substantial mass-loss for Antlia II and Crater II based on offset from the E. N. Kirby et al. (2013) relation. We assign both objects to Class 2 where $f_{\rm bound} \gtrsim 0.2$ is possible, such that the O. Sameie et al. (2020) Antlia II estimate of 0.1 is difficult to match but the J. L. Sanders et al. (2018) Crater II estimate of 0.3 is feasible.

Downloaded from https://academic.oup.com/mnras/article/546/3/stag029/8417159 by guest on 27 February 2026

edge of the satellite mass–metallicity relation, suggesting that this may be near where the intrinsic relation lies. These results imply a difference in the mass–metallicity relations between centrals and satellites, an effect already observed at higher masses (A. Pasquali et al. 2010). Simulators can also be more accepting of a mass–metallicity relation for isolated low-mass galaxies that is lower and steeper than what is observed in the Local Group, since it is the intrinsic relation that they seek to reproduce (e.g. S. Bose & A. J. Deason 2025).

Finally, when estimating the stellar mass of streams a common technique (e.g. T. S. Li et al. 2022) is to measure the stream's metallicity and then adopt a mass–metallicity relation, often from E. N. Kirby et al. (2013). We emulate this method for Auriga systems by computing the mean metallicity of unbound stars and converting this into a stellar mass using the evolved relation (solid line in Fig. 2). We find this underestimates the true total mass with $\log_{10}(M_*^{\rm est}/M_*^{\rm true}) = -0.34^{+0.38}_{-0.59}$ for systems with a progenitor at the present day and $\log_{10}(M_*^{\rm est}/M_*^{\rm true}) = -0.57^{+0.33}_{-0.34}$ for systems with no progenitor. The latter is impacted by redshift evolution of the intrinsic relation (Fig. 1). While this technique is an improvement over methods using star counts for only the chunk of stream that is detected, we recommend such estimates should be considered lower bounds on the total mass of the system.

5 CONCLUDING REMARKS

Accreted systems in Auriga follow established correlations between stellar mass, metallicity, and star formation history (Fig. 1) that, upon accretion and disruption, imprint a tidally evolved mass–metallicity relation that differs from the intrinsic one (Fig. 2). The scatter about this tidally evolved relation is similar to that observed for Local Group satellites (Fig. 3) and offset from the relation predicts which satellites have experienced substantial mass-loss (Fig. 4). The mass–metallicity relation for Local Group satellites is not only compatible with tidal mass-loss, but provides further evidence that a wealth of faint streams awaits discovery in Rubin, *Euclid*, and *Roman* data.

ACKNOWLEDGEMENTS

We thank Astha Chaturvedi, Emma Dodd, Ivanna Escala, Azi Fattahi, Peter Ferguson, and Guilherme Limberg for enlightening discussions, as well as Jess Doppel and Louise Welsh for peer pressure to 'just write the paper' and an anonymous referee for helpful suggestions. This research made extensive use of arXiv.org and NASA's Astrophysics Data System for bibliographic information.

AHR was supported by a fellowship funded by the Wenner Gren Foundation, a Research Fellowship from the Royal Commission for the Exhibition of 1851, and by STFC through grant ST/T000244/1. RB was supported by the UZH Postdoc Grant, grant no. FK-23116 and the SNSF through the Ambizione Grant PZ00P2_223532. FF was supported by a UKRI Future Leaders Fellowship (grant no. MR/X033740/1). FAG acknowledges support from the ANID BASAL project FB210003, from the ANID FONDECYT Regular grants 1251493 and from the HORIZON MSCA-2021-SE-01 Research and Innovation Programme under the Marie Sklodowska-Curie grant agreement number 101086388. RJJG was supported by an STFC Ernest Rutherford Fellowship (ST/W003643/1). FM acknowledges funding from the European Union–NextGenerationEU under the HPC project 'National Centre for HPC, Big Data and Quantum Computing' (PNRR–M4C2–I1.4–CN00000013–CUP J33C22001170001). This work was supported by collaborative visits funded by the Cosmology and Astroparticle Student and Postdoc Exchange Network (CASPEN). We acknowledge support from the DiRAC Institute in the Department of Astronomy at the University of Washington. The DiRAC Institute is supported through generous gifts from the Charles and Lisa Simonyi Fund for Arts and Sciences, Janet and Lloyd Frink, and the Washington Research Foundation.

This work used the DiRAC@Durham facility managed by the Institute for Computational Cosmology on behalf of the STFC DiRAC HPC Facility (www.dirac.ac.uk). The equipment was funded by BEIS capital funding via STFC capital grants ST/K00042X/1, ST/P002293/1, ST/R002371/1, and ST/S002502/1, Durham University, and STFC operations grant ST/R000832/1. DiRAC is part of the National e-Infrastructure. This research used resources of the Argonne Leadership Computing Facility, a U.S. Department of Energy (DOE) Office of Science user facility at Argonne National Laboratory and is based on research supported by the U.S. DOE Office of Science-Advanced Scientific Computing Research Program, under Contract No. DE-AC02-06CH11357.

For the purpose of open access, the author has applied a Creative Commons Attribution (CC BY) licence to any Author Accepted Manuscript version arising from this submission.

SOFTWARE This research made use of the PYTHON programming language, along with many community-developed or maintained software packages including:

(i) ASTROPY (Astropy Collaboration 2013, 2018, 2022),
(ii) CMASHER (E. der Velden 2020; E. Velden et al. 2024)
(iii) CYTHON (S. Behnel et al. 2011)
(iv) H5PY (A. Collette 2013; A. Collette et al. 2022)
(v) JUPYTER (F. Perez & B. E. Granger 2007; T. Kluyver et al. 2016)
(vi) MATPLOTLIB (J. D. Hunter 2007)
(vii) NUMPY (C. R. Harris et al. 2020)
(viii) PANDAS (W. McKinney 2010; T. team 2022)
(ix) SCIKIT-LEARN (F. Pedregosa et al. 2011; L. Buitinck et al. 2013; O. Grisel et al. 2022)
(x) SCIPY (P. Virtanen et al. 2020; R. Gommers et al. 2022).

We also thank the maintainers of the AREPO-SNAP-UTIL package. Parts of the results in this work make use of the colormaps in the CMASHER package. Software citation information aggregated using The Software Citation Station (T. Wagg & F. S. Broekgaarden 2024; T. Wagg, F. Broekgaarden & K. Gültekin 2024).

DATA AVAILABILITY

Halo catalogues, merger trees, and particle data (Section 2) for Auriga are publicly available (detailed in the Auriga project data release; R. J. J. Grand et al. 2024) to download via the Globus platform.[9] The observational data used in this work is compiled in Table B2 largely thanks to the heroic efforts of Andrew Pace and Alan McConnachie (A. W. McConnachie 2012; A. B. Pace 2025).

[9] https://wwwmpa.mpa-garching.mpg.de/auriga/data

Downloaded from https://academic.oup.com/mnras/article/546/3/stag029/8417159 by guest on 27 February 2026

REFERENCES

Agertz O. et al., 2020, MNRAS, 491, 1656
Applebaum E., Brooks A. M., Christensen C. R., Munshi F., Quinn T. R., Shen S., Tremmel M., 2021, ApJ, 906, 96
Asplund M., Amarsi A. M., Grevesse N., 2021, A&A, 653, A141
Astropy Collaboration, 2013, A&A, 558, A33
Astropy Collaboration, 2018, AJ, 156, 123
Astropy Collaboration, 2022, ApJ, 935, 167
Barbosa F. O. et al., 2025, ApJ, 993, 77
Behnel S., Bradshaw R., Citro C., Dalcin L., Seljebotn D. S., Smith K., 2011, Comput. Sci. Eng., 13, 31
Bose S., Deason A. J., 2025, preprint (arXiv:2509.07066)
Buitinck L. et al., 2013, in ECML PKDD Workshop: Languages for Data Mining and Machine Learning. p. 108
Carrera R., Gallart C., Hardy E., Aparicio A., Zinn R., 2008, AJ, 135, 836
Carrillo A., Deason A. J., Fattahi A., Callingham T. M., Grand R. J. J., 2024, MNRAS, 527, 2165
Charles E. J. E. et al., 2023, MNRAS, 521, 3527
Collette A., 2013, Python and HDF5. O'Reilly
Collette A. et al., 2022, h5py/h5py: 3.7.0, Zenodo
Collins M. L. M. et al., 2013, ApJ, 768, 172
Collins M. L. M., Tollerud E. J., Rich R. M., Ibata R. A., Martin N. F., Chapman S. C., Gilbert K. M., Preston J., 2020, MNRAS, 491, 3496
Collins M. L. M. et al., 2021, MNRAS, 505, 5686
Crnojević D. et al., 2014, MNRAS, 445, 3862
Cullinane L. R. et al., 2024, ApJ, 972, 133
Cunningham E. C., Hunt J. A. S., Price-Whelan A. M., Johnston K. V., Ness M. K., Lu Y. L., Escala I., Stelea I. A., 2024, ApJ, 963, 95
de Vaucouleurs G., de Vaucouleurs A., Corwin Herold G. J., Buta R. J., Paturel G., Fouque P., 1991, Third Reference Catalogue of Bright Galaxies
Escala I. et al., 2018, MNRAS, 474, 2194
Escala I. et al., 2025, ApJ, 991, 31
Fattahi A. et al., 2020, MNRAS, 497, 4459
Font A. S., Johnston K. V., Bullock J. S., Robertson B. E., 2006, ApJ, 638, 585
Fragkoudi F. et al., 2020, MNRAS, 494, 5936
Fragkoudi F., Grand R. J. J., Pakmor R., Gómez F., Marinacci F., Springel V., 2025, MNRAS, 538, 1587
Fu S. W. et al., 2023, ApJ, 958, 167
Geha M., Guhathakurta P., Rich R. M., Cooper M. C., 2006, AJ, 131, 332
Genina A., Frenk C. S., Benítez-Llambay A., Cole S., Navarro J. F., Oman K. A., Fattahi A., 2019, MNRAS, 488, 2312
Gómez F. A., White S. D. M., Grand R. J. J., Marinacci F., Springel V., Pakmor R., 2017, MNRAS, 465, 3446
Gommers R. et al., 2022, scipy/scipy: SciPy 1.9.1, Zenodo
Grand R. J. J. et al., 2017, MNRAS, 467, 179
Grand R. J. J. et al., 2021, MNRAS, 507, 4953
Grand R. J. J., Fragkoudi F., Gómez F. A., Jenkins A., Marinacci F., Pakmor R., Springel V., 2024, MNRAS, 532, 1814
Grillmair C. J. et al., 1996, AJ, 112, 1975
Grimozzi S. E., Font A. S., De Rossi M. E., 2024, MNRAS, 530, 95
Grisel O. et al., 2022, scikit-learn/scikit-learn: scikit-learn 1.1.2, Zenodo
Harris C. R. et al., 2020, Nature, 585, 357
Hasselquist S. et al., 2021, ApJ, 923, 172
Hunter J. D., 2007, Comput. Sci. Eng., 9, 90
Ibata R., Irwin M., Lewis G. F., Stolte A., 2001, ApJ, 547, L133
Ji A. P. et al., 2020, AJ, 160, 181
Ji A. P. et al., 2021, ApJ, 921, 32
Kewley L. J., Ellison S. L., 2008, ApJ, 681, 1183
Khoperskov S., Minchev I., Steinmetz M., Marabotto J., Kordopatis G., Delgado Gomez J., Libeskind N., 2023, preprint (arXiv:2310.05287)
Kirby E. N., Simon J. D., Geha M., Guhathakurta P., Frebel A., 2008, ApJ, 685, L43
Kirby E. N., Lanfranchi G. A., Simon J. D., Cohen J. G., Guhathakurta P., 2011, ApJ, 727, 78
Kirby E. N., Cohen J. G., Guhathakurta P., Cheng L., Bullock J. S., Gallazzi A., 2013, ApJ, 779, 102
Kirby E. N., Gilbert K. M., Escala I., Wojno J., Guhathakurta P., Majewski S. R., Beaton R. L., 2020, AJ, 159, 46
Kizhuprakkat N. et al., 2024, MNRAS, 531, 4108
Kluyver T. et al., 2016, in Loizides F., Scmidt B., eds, Positioning and Power in Academic Publishing: Players, Agents and Agendas. IOS Press, Netherlands, p. 87
Kvasova K. A., Kirby E. N., Beaton R. L., 2024, ApJ, 972, 180
Leaman R. et al., 2013, ApJ, 767, 131
Li T. S. et al., 2022, ApJ, 928, 30
Limberg G., Souza S. O., Pérez-Villegas A., Rossi S., Perottoni H. D., Santucci R. M., 2022, ApJ, 935, 109
Limberg G. et al., 2025, preprint (arXiv:2512.02177)
Ma X., Hopkins P. F., Faucher-Giguère C.-A., Zolman N., Muratov A. L., Kereš D., Quataert E., 2016, MNRAS, 456, 2140
Maiolino R., Mannucci F., 2019, A&AR, 27, 3
Mannucci F., Cresci G., Maiolino R., Marconi A., Gnerucci A., 2010, MNRAS, 408, 2115
Marinacci F., Grand R. J. J., Pakmor R., Springel V., Gómez F. A., Frenk C. S., White S. D. M., 2017, MNRAS, 466, 3859
Martin N. F. et al., 2014, ApJ, 793, L14
Martin N. F. et al., 2016, ApJ, 833, 167
McConnachie A. W., 2012, AJ, 144, 4
McConnachie A. W., Irwin M. J., 2006, MNRAS, 365, 1263
McKinney W., 2010, in van der Walt Stéfan, Millman Jarrod eds, Proceedings of the 9th Python in Science Conference. p. 56
Monachesi A. et al., 2019, MNRAS, 485, 2589
Muñoz R. R., Côté P., Santana F. A., Geha M., Simon J. D., Oyarzún G. A., Stetson P. B., Djorgovski S. G., 2018, ApJ, 860, 66
Naidu R. P. et al., 2022, preprint (arXiv:2204.09057)
Niederste-Ostholt M., Belokurov V., Evans N. W., Peñarrubia J., 2010, ApJ, 712, 516
Orkney M. D. A. et al., 2023, MNRAS, 525, 683
Pace A. B., 2025, Open J. Astrophys., 8, 142
Pace A. B. et al., 2020, MNRAS, 495, 3022
Pakmor R., Springel V., Bauer A., Mocz P., Munoz D. J., Ohlmann S. T., Schaal K., Zhu C., 2016, MNRAS, 455, 1134
Pakmor R. et al., 2017, MNRAS, 469, 3185
pandas development team T., 2022, pandas-dev/pandas: Pandas, Zenodo
Parisi M. C., Geisler D., Grocholski A. J., Clariá J. J., Sarajedini A., 2010, AJ, 139, 1168
Pasquali A., Gallazzi A., Fontanot F., van den Bosch F. C., De Lucia G., Mo H. J., Yang X., 2010, MNRAS, 407, 937
Pathak D., Christensen C. R., Brooks A. M., Munshi F., Wright A. C., Carter C., 2025, ApJ, 989, 178
Pedregosa F. et al., 2011, J. Mach. Learn. Res., 12, 2825
Perez F., Granger B. E., 2007, Comput. Sci. Eng., 9, 21
Rhode K. L. et al., 2023, AJ, 166, 180
Richardson J. C. et al., 2011, ApJ, 732, 76
Riley A. H. et al., 2025, MNRAS, 542, 2443 (Paper I)
Robertson B., Bullock J. S., Font A. S., Johnston K. V., Hernquist L., 2005, ApJ, 632, 872
Sameie O., Chakrabarti S., Yu H.-B., Boylan-Kolchin M., Vogelsberger M., Zavala J., Hernquist L., 2020, preprint (arXiv:2006.06681)
Sanders J. L., Evans N. W., Dehnen W., 2018, MNRAS, 478, 3879
Schaye J. et al., 2015, MNRAS, 446, 521
Shipp N. et al., 2023, ApJ, 949, 44
Shipp N. et al., 2025, MNRAS, 542, 1109 (Paper II)
Simon J. D., 2019, ARA&A, 57, 375
Simon J. D., Geha M., 2007, ApJ, 670, 313
Simpson C. M., Grand R. J. J., Gómez F. A., Marinacci F., Pakmor R., Springel V., Campbell D. J. R., Frenk C. S., 2018, MNRAS, 478, 548
Slater C. T., Bell E. F., Martin N. F., Tollerud E. J., Ho N., 2015, ApJ, 806, 230

Downloaded from https://academic.oup.com/mnras/article/546/3/stag029/8417159 by guest on 27 February 2026

Springel V., 2010, MNRAS, 401, 791
Springel V., White S. D. M., Tormen G., Kauffmann G., 2001, MNRAS, 328, 726
Taibi S., Battaglia G., Leaman R., Brooks A., Riggs C., Munshi F., Revaz Y., Jablonka P., 2022, A&A, 665, A92
Torrealba G., Koposov S. E., Belokurov V., Irwin M., 2016, MNRAS, 459, 2370
Torrey P. et al., 2019, MNRAS, 484, 5587
Tremonti C. A. et al., 2004, ApJ, 613, 898
van der Velden E., 2020, J. Open Source Softw., 5, 2004
van der Velden E., Robert C., Batten A., Clauss C., beskep (Daniel) H., Thyng K., 2024, 1313e/CMasher: v1.8.0, Zenodo
Virtanen P. et al., 2020, Nat. Methods, 17, 261
Vivas A. K., Walker A., Martínez-Vázquez C., Cooke M., Gallart C., Monelli M., Rojas Cancino J. A., Nidever D., 2025, preprint (arXiv:2512.05535)
Wagg T., Broekgaarden F. S., 2024, preprint (arXiv:2406.04405)
Wagg T., Broekgaarden F., Gültekin K., 2024, TomWagg/software-citation-station: v1.2, Zenodo
Wojno J., Gilbert K. M., Kirby E. N., Escala I., Beaton R. L., Tollerud E. J., Majewski S. R., Guhathakurta P., 2020, ApJ, 895, 78

APPENDIX A: IGNORING METALLICITY GRADIENTS

Many of the key results in this analysis for Auriga are driven simultaneously by both tidal mass-loss and by initial negative radial metallicity gradients. Due to these gradients, low metallicity stars are preferentially lost from the outskirts, raising the mean metallicity of the bound progenitor. While we prefer to present results that include both effects, it can be interesting to see if our results qualitatively hold when ignoring the effect of radial gradients.

In Fig. A1, we show a version of Fig. 2 that ignores the metallicity evolution of the bound progenitor by adopting the metallicity of the total system. In other words, individual points move exclusively to lower stellar mass. We still find that the mean relation moves away from the intrinsic one, the scatter about the relation increases, and that individual points 'invert' their relationship to the relation.

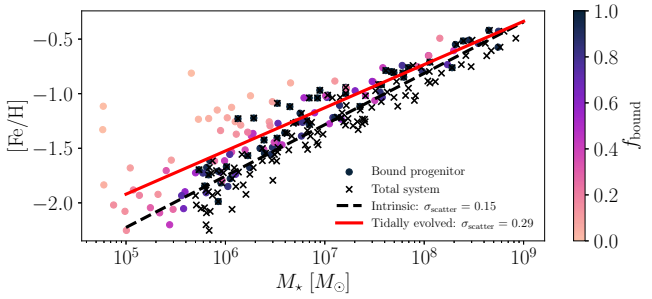

Figure A1. Similar to Fig. 2 but excluding the effect of radial metallicity gradients.

APPENDIX B: DISRUPTION PREDICTION FOR OBSERVED SATELLITES

In Section 3, we introduce a broad classification for how disrupted Auriga satellites are, based on their offset from the tidally evolved mass–metallicity relation Δ[Fe/H] normalized by the scatter about the relation $\sigma_{\rm scatter}$. The exact boundaries are listed in Table B1 and separate into the following qualitative descriptions:

(i) Class 1: unlikely to have experienced any mass-loss
(ii) Class 2: mass-loss down to $f_{\rm bound} \sim 0.2$ is possible but disfavoured
(iii) Class 3: substantial mass-loss is favoured, with most satellites having $0.05 < f_{\rm bound} < 0.8$
(iv) Class 4: no intact satellites, $f_{\rm bound} < 0.2$ strongly preferred
(v) Class 5: no intact satellites, only $f_{\rm bound} < 0.05$

Table B1 also lists quantitative metrics for how disrupted Auriga satellites are in each Class. As shown in Fig. 4, both the highest level of disruption that is possible and the fraction of satellites that are substantially disrupted increase with ascending Class order. We caution that these predictions are less robust for systems that have recent star formation (see final paragraph of Section 3).

We then apply the same exercise to the observed Local Group satellites to predict how much tidal disruption they have experienced. We begin with compilations of their stellar masses and mean metallicities (Fig. 3), then fit a relation in the same manner as done for the Auriga satellites. Our fit takes the following form

$$[\mathrm{Fe/H}] = -1.80 + 0.35 \log_{10}\left(\frac{M_\star}{10^6\ \mathrm{M}_\odot}\right) \quad \text{(B1)}$$

The equivalent for E. N. Kirby et al. (2013), taking the luminosity–metallicity relation reported in their equation (3) and assuming $M/L_V = 2$, is

$$[\mathrm{Fe/H}] = -1.77 + 0.29 \log_{10}\left(\frac{M_\star}{10^6\ \mathrm{M}_\odot}\right) \quad \text{(B2)}$$

We compute each satellite's offset from the relation (equation B1) normalized by the reported scatter ($\sigma_{\rm scatter} = 0.23$). These are then directly compared to the Class boundary definitions in Table B1. The stellar masses, metallicities, offsets from the relation in equation (B1), and resulting Class assignments are indicated in Table B2. We note that Local Group satellites with detected tidal tails are typically in Classes 3–5 (Sagittarius, NGC 147, And XIX, And XXI; R. Ibata et al. 2001; D. Crnojević et al. 2014; M. L. M. Collins et al. 2020, 2021), with some in Class 2 (Antlia II, Crater

Table B1. Properties of the different broad categories of disruption assigned to individual satellites. We provide the Class number, boundary definitions (see Section 4 and Fig. 4), the distribution of $f_{\rm bound}$ for Auriga satellites, fraction of Auriga satellites that are intact ($f_{\rm bound} > 0.97$, see Paper I, Paper II), fraction of Auriga satellites with $f_{\rm bound} < 0.8$, and number of Milky Way and M31 satellites in this Class.

Class	Definition Δ[Fe/H]/$\sigma \in$	$f^{\rm Au}_{\rm bound}$	$F^{\rm Au}_{\rm intact}$	$F^{\rm Au}_{<0.8}$	$N^{\rm obs}_{\rm sat}$
1	$(-\infty, -1]$	$0.92^{+0.07}_{-0.46}$	0.38	0.31	5
2	$(-1, 0]$	$0.81^{+0.18}_{-0.43}$	0.21	0.47	17
3	$(0, 1]$	$0.39^{+0.42}_{-0.26}$	0.07	0.83	12
4	$(1, 2]$	$0.06^{+0.05}_{-0.02}$	0.00	1.00	3
5	$(2, \infty)$	$0.00^{+0.01}_{-0.00}$	0.00	1.00	2

Downloaded from https://academic.oup.com/mnras/article/546/3/stag029/8417159 by guest on 27 February 2026

Table B2. Observational data (compiled by A. B. Pace 2025) presented in Fig. 3 along with the vertical offset from the mass–metallicity relation (Δ[Fe/H]) and a Class indicating the potential level of (tidal) disruption experienced by the system (see the text in Appendix B for details). We also list references for each measurement, which correspond to the following citations: (1) A. P. Ji et al. (2021), (2) R. R. Muñoz et al. (2018), (3) J. D. Simon (2019), (4) G. Torrealba et al. (2016), (5) G. Vaucouleurs et al. (1991), (6) R. Carrera et al. (2008), (7) A. W. McConnachie (2012), (8) M. C. Parisi et al. (2010), (9) A. B. Pace et al. (2020), (10) N. F. Martin et al. (2016), (11) E. N. Kirby et al. (2020), (12) J. Wojno et al. (2020), (13) A. W. McConnachie & M. J. Irwin (2006), (14) M. L. M. Collins et al. (2013), (15) K. A. Kvasova, E. N. Kirby & R. L. Beaton (2024), (16) L. R. Cullinane et al. (2024), (17) M. L. M. Collins et al. (2021), (18) E. J. E. Charles et al. (2023), (19) J. C. Richardson et al. (2011), (20) C. T. Slater et al. (2015), (21) K. L. Rhode et al. (2023), (22) N. F. Martin et al. (2014), (23) E. N. Kirby et al. (2013).

Name	$\log_{10}(M_\star/M_\odot)$	[Fe/H]	Δ[Fe/H]	Class	References
		Milky Way satellites			
Antlia II	6.13	−1.9	−0.15	2	[1,1]
Canes Venatici I	5.73	−1.91	−0.02	2	[2,3]
Carina	6.01	−1.8	−0.0	2	[2,3]
Crater II	5.51	−2.16	−0.19	2	[4,1]
Draco	5.78	−2.0	−0.13	2	[2,3]
Fornax	7.59	−1.07	0.18	3	[2,3]
Leo I	6.96	−1.48	−0.02	2	[2,3]
Leo II	6.12	−1.68	0.08	3	[2,3]
LMC	9.46	−0.5	0.1	3	[5,6]
Sagittarius	7.63	−0.53	0.7	5	[7,3]
Sculptor	6.54	−1.73	−0.12	2	[2,3]
Sextans	5.72	−1.97	−0.08	2	[2,3]
SMC	8.95	−1.0	−0.22	2	[5,8]
Ursa Minor	5.78	−2.13	−0.26	1	[2,9]
		M31 satellites			
Andromeda I	6.77	−1.51	0.02	3	[10,11]
Andromeda II	6.92	−1.47	0.01	3	[10,12]
Andromeda III	6.03	−1.75	0.04	3	[10,11]
Andromeda V	5.95	−1.84	−0.03	2	[10,11]
Andromeda VI	6.75	−1.5	0.04	3	[13,14]
Andromeda VII	7.35	−1.37	−0.04	2	[13,11]
Andromeda IX	5.69	−2.03	−0.12	2	[10,12]
Andromeda XIV	5.69	−2.23	−0.33	1	[10,12]
Andromeda XV	5.58	−1.43	0.51	5	[10,12]
Andromeda XVII	5.35	−1.7	0.32	4	[10,14]
Andromeda XVIII	5.9	−1.53	0.3	4	[10,15]
Andromeda XIX	6.25	−1.5	0.21	3	[10,16]
Andromeda XXI	5.81	−1.7	0.16	3	[10,17]
Andromeda XXIII	6.14	−2.2	−0.45	1	[10,14]
Andromeda XXV	5.87	−1.9	−0.06	2	[10,18]
Andromeda XXVII	5.39	−2.1	−0.09	2	[19,14]
Andromeda XXVIII	5.64	−1.84	0.08	3	[20,20]
Andromeda XXIX	5.5	−1.9	0.07	3	[20,20]
Cassiopeia II	5.33	−1.7	0.33	4	[10,14]
Cassiopeia III	7.19	−1.7	−0.32	1	[21,22]
Lacerta I	6.72	−2.0	−0.45	1	[21,22]
NGC 147	8.17	−0.83	0.22	3	[7,23]
NGC 185	8.18	−1.12	−0.08	2	[7,23]
NGC 205	8.84	−0.92	−0.1	2	[7,23]
Perseus I	5.78	−2.0	−0.13	2	[21,22]

II, NGC 205; M. Geha et al. 2006; A. P. Ji et al. 2021; G. Limberg et al. 2025; A. K. Vivas et al. 2025).

We note that there are three M31 satellites (M 32, IC 10, and LGS 3) brighter than $M_V = -7.7$ omitted from our analysis because they lack literature spectroscopic metallicities in the compilations we consider. The available isochrone or RGB colour metallicities compiled by A. W. McConnachie (2012) suggest that IC 10 and LGS 3 are not candidates for heavy disruption under our framework (Class 1 or 2 depending on the adopted relation). However, the available data for M 32 gives it a very high metallicity ([Fe/H] = −0.25; C. J. Grillmair et al. 1996) for its stellar mass. This would place M 32 in Class 5, comparable to Sagittarius (see also I. Escala et al. 2025).

This paper has been typeset from a TEX/LATEX file prepared by the author.

© The Author(s) 2026.
Published by Oxford University Press on behalf of Royal Astronomical Society. This is an Open Access article distributed under the terms of the Creative Commons Attribution License (https://creativecommons.org/licenses/by/4.0/), which permits unrestricted reuse, distribution, and reproduction in any medium, provided the original work is properly cited.

Downloaded from https://academic.oup.com/mnras/article/546/3/stag029/8417159 by guest on 27 February 2026